An Evaluation of Probable Bedrock Exposure in the Sinus Meridiani Region of the Martian Highlands

J. R. Zimbelman and R. A. Craddock

Center for Earth and Planetary Studies, National Air and Space Museum,
Smithsonian Institution, Washington, DC 20560

The study region (15°N to 15°S, 330° to 360°W) includes portions of the classical low-albedo regions of Sinus Meridiani and Sinus Sabaeus and the high-albedo region of Arabia and is entirely within the cratered highlands of Mars. This region has been the subject of several spectral reflectance studies and it is also included in global studies at thermal infrared and radar wavelengths. More than 400 high-resolution (8-36 m/pixel) Viking images in the study area were used to estimate the percentage of the area of each frame having locally steep slopes, here assumed to be the most probable locality for exposure of bedrock. Forty-two percent of the high-resolution frames have <1% probable bedrock exposure while 3% of the frames have 15% probable bedrock exposure, the maximum observed value. Rims of young impact craters and scarps account for most of the bedrock exposure locations. Eroded layers of competent material compose the majority of steep slopes at some locations in low-albedo areas (e.g., 0° to 8°N, 350° to 360°W); these locations are also associated with local enhancements of thermal inertia that may be related to surface exposures of indurated sediments. There is no significant difference in probable bedrock exposure between high-albedo and low-albedo regions, and there is no apparent correlation between bedrock exposure and the units defined by either spectral reflectance studies or photogeologic mapping. These results indicate that great caution must be exercised in attributing remotely sensed properties to bedrock materials.

INTRODUCTION

A major goal of remote-sensing studies of Mars is to obtain constraints on the physical properties and composition of bedrock materials. The study of *in situ* bedrock, as opposed to loose rocks and soil on the surface, is important because the outcrops provide a window into the underlying geologic units and structures, both of which provide valuable clues to the geologic history of the entire region. The composition and physical condition of the bedrock also determine the effectiveness of various physical or chemical weathering processes and the products that result from the breakdown of the bedrock materials. Future missions to the martian surface, such as an unmanned rover or a manned expedition, will include sample collection, and it is crucial that these missions be able to sample bedrock materials wherever possible. Unfortunately, the active aeolian environment and the ubiquitous presence of dust on Mars make identification of bedrock exposures difficult at best, and perhaps even impossible at certain locations. The work described here provides estimates of the amount of probable bedrock exposures visible in the highest-resolution Viking imaging data for a selected region of the martian surface. The results obtained from the image data represent an independent means for evaluating the possible contribution of bedrock to remote-sensing measurements of Mars.

BACKGROUND

Remote-sensing techniques provide our only means at present for obtaining direct information about the physical and chemical make-up of the martian surface. Synthesis of multiple data types has been particularly valuable in regional studies on the terrestrial planets, including the Earth (*Sabins,* 1978, pp. 385-400), the Moon (*Thompson et al.,* 1974, 1980), and Mars (*Schaber,* 1980; *Mouginis-Mark et al.,* 1980; *Zimbelman and Greeley,* 1981; *Presley and Arvidson,* 1988). The great advantage of using more than one wavelength of the electromagnetic spectrum is that different wavelengths are sensitive to surface conditions at different scales. Thus, different wavelength regions can often provide complementary views of the surface being studied.

Viking Orbiter images taken through various color filters have been used to delineate many surface spectral units on Mars, some of which could have important compositional implications (*Soderblom et al.,* 1978; *McCord et al.,* 1982; *Arvidson et al.,* 1982; *Presley and Arvidson,* 1988). Earth-based spectral observations have revealed a variety of probable and possible constituents of the martian soil including ferric oxides, oxidized basaltic weathering products, and other possible ferrous minerals (*Adams and McCord,* 1969; *Singer et al.,* 1979; *Singer,* 1982; *Morris et al.,* 1990; *Bell et al.,* 1990). Typically these studies have lacked the spatial resolution to relate the measurements to a specific unit or feature on the martian surface. The work presented here is complementary to these analyses, providing information that will better constrain the geologic significance of the reflectance properties.

Visual images represent a unique part of remote-sensing data since the morphology and texture of surface features provide important clues to the surface history. Interpreting the surface history is particularly important at locations where differing degrees of erosion or deposition can be observed (*Carr,* 1981, p. 165). High-resolution images are important for assessing the processes active on the martian surface because significant features may be visible at 10-m/pixel resolution, but the same features may be indistinguishable at >50-m/pixel resolution (*Zimbelman,* 1987). Even though atmospheric conditions moderate the fine textural detail visible in the Viking images (*Kahn et al.,* 1986), diagnostic morphologic information can

often be found in the highest-resolution images; a few examples include aeolian depositional features (*Breed et al.*, 1987; *Zimbelman*, 1987), erosion of ejecta around craters in volatile-rich targets (*Mouginis-Mark*, 1987), fine-scale fluvial erosion (*Scott and Chapman*, 1989), and multilayered deposits on the northern plains (*Zimbelman et al.*, 1989). These and other processes act to diminish the exposure of bedrock materials observable by any remote-sensing technique. Geologic interpretation of remote-sensing results should thus be augmented by a process-related evaluation of high-resolution (preferably <30 m/pixel) images.

The Viking Infrared Thermal Mapper (IRTM) experiment measured the thermal infrared emission of the planet in five wavelength bands, along with broadband reflected energy at visual wavelengths (*Kieffer et al.*, 1977). These data were used to provide global maps of broadband surface reflectance (*Kieffer et al.*, 1977; *Pleskot and Miner*, 1981) and thermal properties related to the particle size and/or competence of the martian soil (*Kieffer et al.*, 1977; *Zimbelman and Kieffer*, 1979; *Palluconi and Kieffer*, 1981; *Christensen*, 1986a; *Jakosky and Christensen*, 1986). The IRTM spectral bands provide useful information on the global distribution of competent material at scales smaller than an individual temperature measurement. The unresolved competent material is interpreted to be individual rocks and "blocks" with an effective diameter of approximately 15 cm (*Christensen*, 1982, 1986b) or indurated sediments, also called "duricrust" (*Jakosky and Christensen*, 1986). Thermal infrared measurements at multiple wavelengths indicate that from 5% to 20% of the martian surface consists of these competent materials, with the low-albedo regions generally having somewhat more competent material at the surface than the high-albedo regions (*Christensen*, 1986b). All the above studies are primarily global in extent, with best resolutions of roughly 60 × 60 km at the equator. Individual IRTM sequences with a resolution of 2 × 5 km have been useful in addressing problems related to individual geologic features or units (*Zimbelman and Greeley*, 1981, 1982; *Christensen*, 1986b; *Zimbelman*, 1986; *Craddock*, 1987; *Zimbelman and Leshin*, 1987).

APPROACH

The location chosen for this study (15°N to 15°S, 330° to 360°W) includes portions of the classical low-albedo regions of Sinus Meridiani and Sinus Sabaeus and the high-albedo region of Arabia and is entirely within the cratered highlands of Mars (Fig. 1). This region was selected because it has been the subject of several studies of spectral reflectance properties at visual wavelengths (*Soderblom et al.*, 1978; *McCord et al.*, 1982; *Arvidson et al.*, 1982; *Presley and Arvidson*, 1988; *Strickland*, 1989), all of which identified units with distinct color characteristics. These studies concluded that the low-albedo regions are "less" obscured by the ubiquitous martian dust than the high-albedo regions, so that low-albedo areas could contain a higher proportion of materials directly related to the local geology. However, the dark materials at many locations on Mars are composed of mobile materials (*Christensen and Kieffer*, 1979; *Peterfreund*, 1981; *Christensen*, 1983; *Thomas*, 1984) so that the possible relation to the local geology may indeed be just as confusing for dark soils

as it is for the bright dust. Geologic maps of the study area delineate regionally extensive units that are interpreted to be among the oldest materials present at the martian surface (*King*, 1977; *Scott and Carr*, 1978; *Moore*, 1980; *Greeley and Guest*, 1987). Both the geologic unit boundaries and the individual reflectance units have distinctive contacts that can be related to features visible in the imaging data.

Presley and Arvidson (1988) used visual and thermal infrared data to evaluate the efficiency of mixing between various regionally transported and more locally derived units. They infer that the surficial units exposed in western Arabia and Sinus Meridiani are mixed aeolian deposits that are essentially decoupled from the underlying bedrock. Thus, bedrock exposures likely will be small compared to the scale of the data used in the *Presley and Arvidson* (1988) study, which varied in resolution from hundreds of meters to kilometers. The present study uses high-resolution imaging and thermal infrared data to assess the abundance of probable bedrock exposures that may be smaller in size than those resolvable in previous studies.

It is important that a functional description of locations with probable bedrock exposure be established for use in the analysis of the high-resolution images. Bedrock is defined as "the solid rock underlying the soil and other unconsolidated materials, or appearing at the surface where these [unconsolidated materials] are absent" (*Webster's Dictionary*, 1971, p. 196). For Mars, the "solid" material underlying the soil could include both competent bedrock and indurated sediments that are mechanically competent and more efficient heat conductors than the unconsolidated soils (*Ditteon*, 1982; *Jakosky and Christensen*, 1986). The Viking Orbiter images do not have sufficient resolution to identify specific features *diagnostic* of exposed bedrock; even at the Viking landing sites some areas of possible bedrock can also be interpreted as the exposed surface of buried boulders (*Sharp and Malin*, 1984). In the absence of conclusive indicators of bedrock, the Orbiter images still provide valuable constraints on the distribution of locations with a high probability of including exposed competent materials.

Locations with the least likelihood of having an overlying accumulation of unconsolidated materials would seem to have the greatest probability of including exposures of competent bedrock materials. Steep slopes (exceeding the angle of repose for particulates and blocks) will shed most unconsolidated materials downslope through gravity-driven mass-wasting, thus providing a surface that might be expected to include exposures of the underlying competent bedrock. This principle was clearly demonstrated at the Hadley Rille on the Moon during the Apollo 15 mission (Fig. 2). Photographs from orbit show steep cliffs along both rims of the rille (Fig. 2a,c), which observations on the ground confirmed to be horizontally layered, vertically jointed massive units of the mare basalt flows (Fig. 2b).

The bedrock outcrops at the Hadley Rille were confined to the upper 60 m of the 400-m-deep rille because talus accumulations completely obscured the lower slopes (*Swann et al.*, 1972). It is significant that the exposures in the Hadley Rille were the *largest* in-place outcrops of lunar rock strata observed during the entire period of Apollo surface explora-
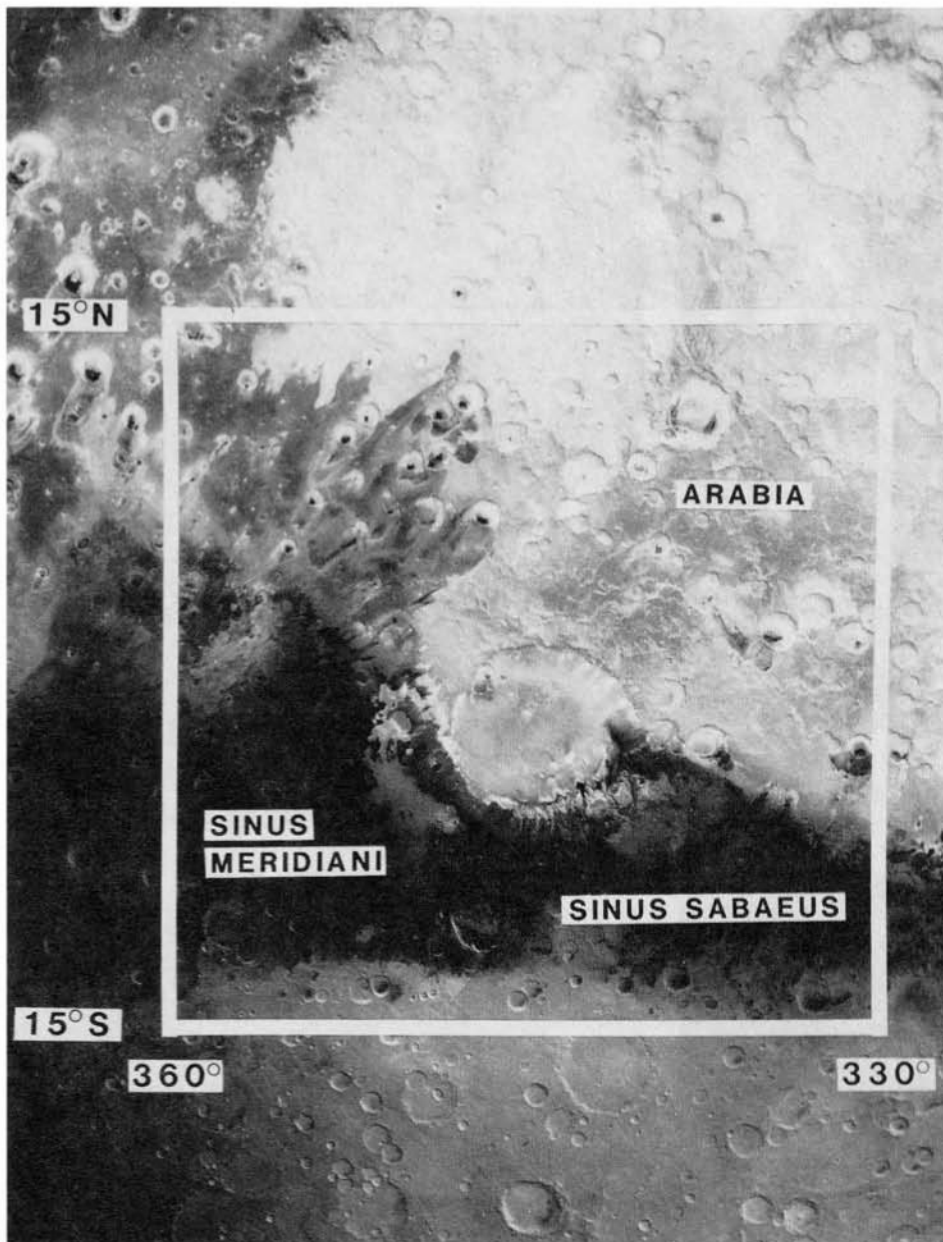
Fig. 1. Study area in the cratered highlands of the Sinus Meridiani region on Mars. Major albedo features are labeled. Image is portion of color mosaic described in *McEwen* (1987).

tion (*Wilhelms*, 1984, p. 184), primarily due to the widespread development of the lunar regolith. The martian atmosphere will eliminate micrometeoroid erosion, but aeolian processes would seem to be more than adequate to supply abundant fine materials for incorporation into an impact-generated regolith on Mars that would tend to bury bedrock at most locations. The lunar results suggest that steep slopes have the best possibility of including bedrock exposures at scales potentially observable from orbit, and here we use this principle as a basic assumption in our observations.

We looked for morphologic evidence of a sharp break in slope in the high-resolution images, coupled with any textural difference between the slope and the surrounding terrain (in order to eliminate the likelihood of a thick blanket of material

over the entire area). The degree of "steepness" was not examined quantitatively, which would have required extensive photoclinometric measurements on hundreds of frames, but rather by relationship to surrounding terrains; changes in slope that appeared to exceed height/width ratios of 1 (equivalent to 45° local slope, which exceeds typical values for the angle of repose) were considered to be "steep" for the purpose of minimizing soil cover. All locations possessing steep slopes were assumed to be candidate sites for possible bedrock exposures. It is likely that some picture elements include mixtures of competent materials and aeolian dust or sand so that the results obtained from the images should be considered as representative of the amount of probable bedrock exposure on scales larger than tens of meters.
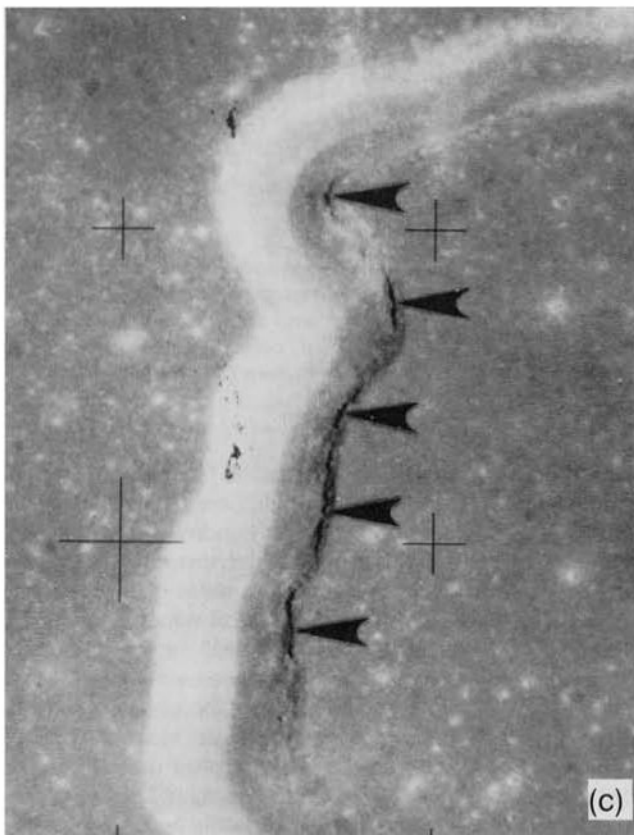
Fig. 2. Bedrock exposures observed on the Moon during the Apollo 15 mission. **(a)** View of Hadley Rille from orbit. Arrows indicate locations of views in parts **(b)** and **(c)**. Apollo photograph AS15-M3-1677. **(b)** Eastern wall of Hadley Rille as viewed by the astronauts on the western rim of the rille. The bedrock exposures (arrows) form steep cliffs near the rim of the rille; horizontal layering and vertical jointing are clearly evident. Exposure has about 8 m of vertical relief. Beneath the exposure the rille wall is covered by talus blocks and fine debris. Apollo Hasselblad photograph AS15-89-12053. **(c)** Orbital view of southern portion of Hadley Rille, with bedrock exposures expressed as steep cliffs along both rims of the rille. Irregular black spots are blemishes on original photograph. Apollo Hasselblad photograph AS15-81-10897.
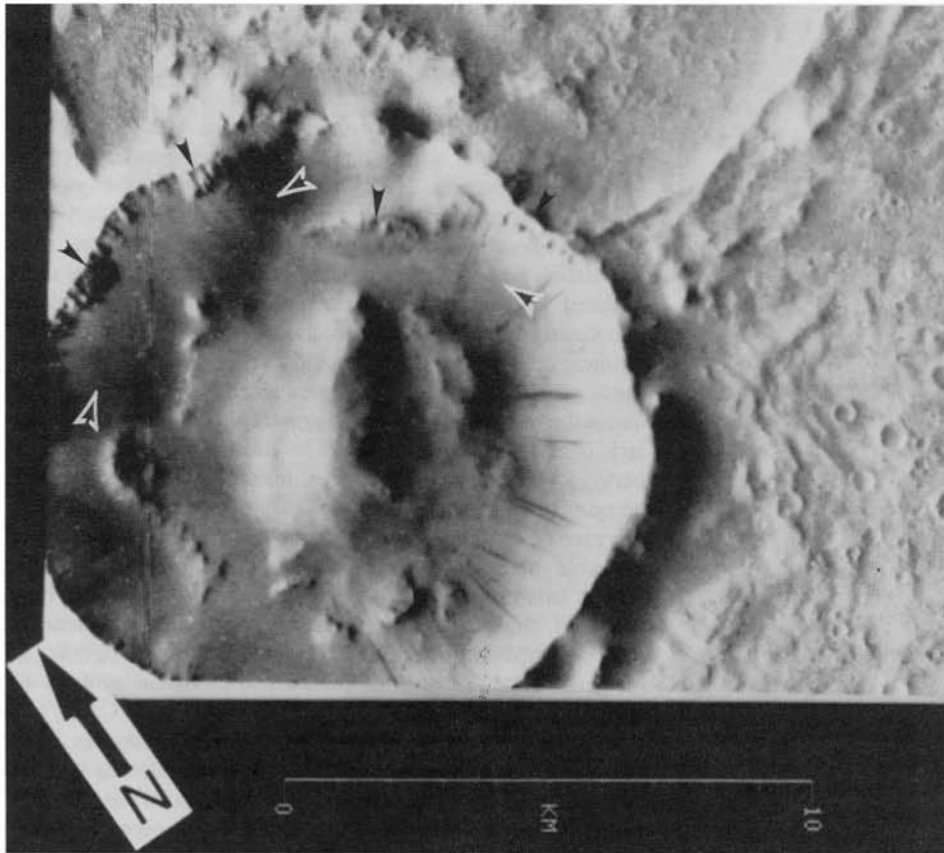
Fig. 3. Example of probable bedrock exposure (solid arrows) on the upper portion of inner walls of a fresh impact crater. Below the exposures are smooth-textured slopes (bordered arrows) that are likely composed of talus accumulations, with individual blocks too small to be resolved in this image. Some of the smooth-textured surfaces have dark streaks extending downslope, where bright dust may have been locally removed by downslope movement along a talus slope (*Moncrief and Williams,* 1989). Viking Orbiter frame 748A12, centered at 1.8°S, 343.9°W, 17-m/pixel resolution.

The procedure adopted for recording the results of our analysis was to obtain a visual estimate of the amount of area within each frame that included steep slopes where bedrock might be present. By comparison with standard petrographic charts for modal abundances within a prescribed area (e.g., *Best,* 1982, p. 597), we independently chose a number for the areal coverage of steep slope locations and averaged the result. If estimates differed by 2-5%, we discussed what each observer was including in the estimate and repeated the procedure. This provided a way of checking the consistency of the observations throughout the entire dataset, and we believe our estimates are reproducible within 5% for frames with 5-15% probable bedrock exposure, and within 2% for frames with <5% exposure, where visual estimates can be more finely discriminated.

Interior walls of impact craters provided the most numerous examples of steep slopes of competent material (Fig. 3, solid arrows). However, even the best images have smooth-textured surfaces covering the majority of the crater interiors (Fig. 3, open arrows), areas that probably consist of talus with individual blocks too small to be resolved and that also may be mantled by dust. Some of the smooth-textured surfaces have dark streaks extending downslope, where bright dust may have been locally removed by downslope movement along a talus slope (*Moncrief and Williams,* 1989). Areas likely dominated by the accumulation of mass-wasting products were not considered good candidate locations for probable bedrock

exposure and they were excluded from our estimates. Walls of channels and other prominent scarps provided additional sites of local steep slopes for probable bedrock exposure.

Broad areas of the study region displayed very few slopes where bedrock might be essentially free of overlying unconsolidated materials (Fig. 4). The presence of features such as sharp-rimmed craters makes it highly unlikely that atmospheric particulates (e.g., *Kahn et al.,* 1986) are responsible for the subdued topography. Differences in the modulation transfer functions for the four cameras on the Viking orbiters could contribute to variations in perceived topography when making comparisons between separate imaging sequences; however, whenever surface detail on the scale of several pixels could be discerned in frames of a particular sequence, we concluded that the subdued appearance was a true surface characteristic. Our observations are quite consistent with the results of *Arvidson et al.* (1982, their Fig. 11), who looked at the same Viking images to determine the relative degree of mantling of the surface. These considerations strengthen the probability that unconsolidated surface sediments dominate nearly the entire scene in areas such as the example shown in Fig. 4.

RESULTS

We examined over 400 high-resolution Viking images within the study area (Table 1), visually estimating the percentage of the area of each frame having a probable exposure of bedrock.
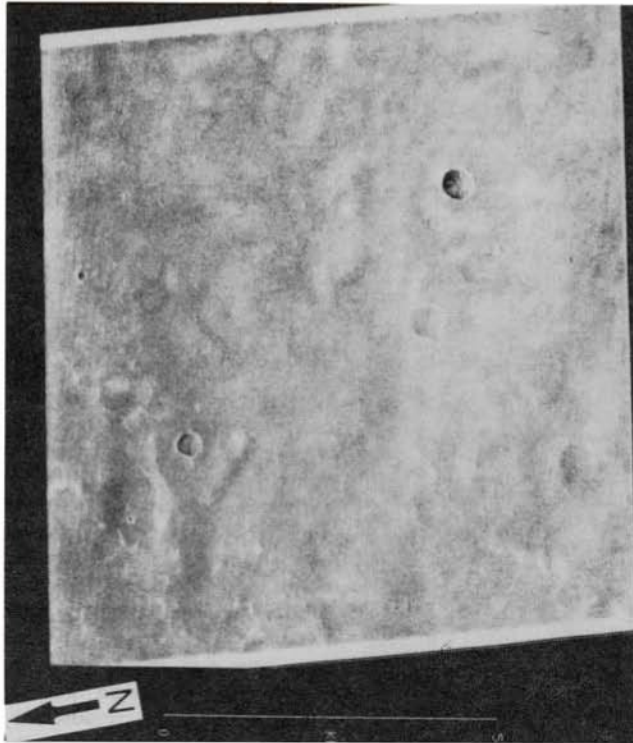
Fig. 4. Example of surface that has greatly subdued topography but still displays a few small craters with sharp rim crests. The sharp-rimmed craters make it unlikely that atmospheric haze is the cause of the subdued topography at this location. Area of probable bedrock exposure is <1% in this frame. Viking Orbiter frame 575B83, centered at 10.6°N, 333.5°W, 8-m/pixel resolution.

the highest image resolution available, since features that appear very rugged at low resolution (Fig. 6a) may have relatively limited areas with steep slopes when viewed at high resolution (Fig. 6b).

The high-resolution images cover about 10% of the total study area (Fig. 7), but they appear to be representative of the region as a whole. There is no significant difference in probable bedrock exposure between high-albedo and low-albedo regions (compare Figs. 1 and 7), and no consistent correlation between probable bedrock exposure and the units defined by spectral reflectance studies. This result is particularly important for low-albedo regions where the low reflectance has been taken to indicate the lack of significant dust cover and, consequently, an enhanced abundance of rocks and soil composed of low-albedo materials (*Pieters*, 1989). The lack of any significant increase in the probable exposure of bedrock within low-albedo regions suggests that the low albedo is at best due to bedrock-derived products, not increased exposure of dark bedrock outcrops. Occurrences of probable bedrock exposure are localized around relatively recent landforms, where impact or tectonic processes have modified the surface subsequent to the emplacement of regional plains units. Such events, either endogenic or exogenic in nature, are not confined to particular geologic or spectral reflectance units.

In addition to an association with recent landforms, steep slopes were also observed at the margin of materials that appear to be both easily eroded and superposed on the surrounding terrain (Fig. 8). The eroded layers seem to result from depositional events that range from local to regional scales. These materials appear to be more competent than unconsolidated aeolian dust and it seems unlikely that they
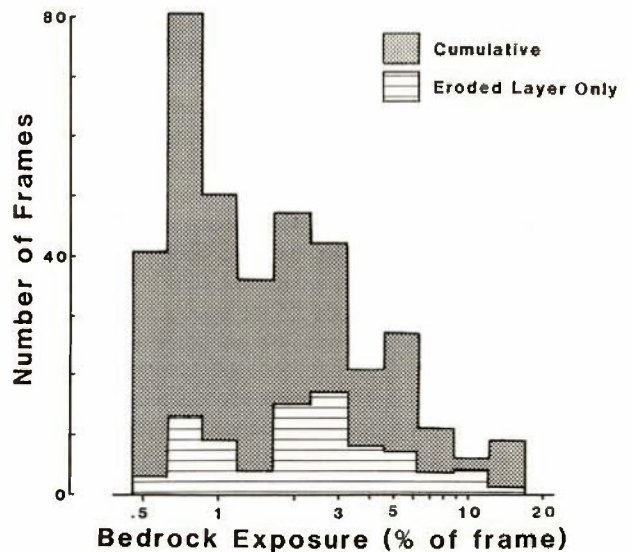
TABLE 1. High-resolution (8–36 m/pixel) Viking orbiter images used for bedrock exposure estimates within the Sinus Meridiani study area.

Viking Orbiter Frame Numbers	
436A52-74	392B01-20
709A01-48	409B17-40
746A48,51-68	410B01-21,29-39
747A31-58	411B01-32,67-98
748A01-16,21-42	413B25-32
749A07-30	416B34-35
826A21-44,51-74	572B67-76
	575B61-76,81-88

Additional high-resolution frames are present within the study area, but they were excluded from this study due to a lack of visible surface detail caused either by abundant atmospheric particulates or extensive data transmission dropouts.

The images examined have resolutions of 8–36 m/pixel, so features smaller than several tens of meters in dimension could not be identified. The entire image set provided the following results: 42% of the high-resolution frames have <1% probable bedrock exposure while 3% of the frames have 15% probable bedrock exposure, the maximum observed value (Fig. 5, dotted pattern). The results emphasize the importance of using

Fig. 5. Distribution of probable bedrock exposures for the entire study area. Bedrock exposure is expressed as the percentage of the frame area. Dotted pattern is the cumulative distribution for all frames; lined pattern is distribution of competent eroded layers only.

Fig. 6. Comparison of rugged terrain viewed at differing image resolutions. **(a)** Wall of a relatively fresh-appearing impact crater imaged at 228-m/pixel resolution. Arrow and box show the location of part **(b)**. Viking Orbiter frame 618A09, centered at 8.3°S, 336.8°W. **(b)** Wall of crater imaged at 11-m/pixel resolution. Note that the occurrence of likely outcrops of competent bedrock are confined to upper slopes of the interior wall of the crater (arrows). Viking Orbiter frame 575B69, centered at 10.0°S, 335.5°W.

have been locally derived; the individual layers may represent a global-scale resurfacing event from early in the history of Mars (*Craddock and Maxwell,* 1990) or they may reflect more recent climatically driven changes in dust deposition and consolidation (*Christensen,* 1986a). The eroded layers are most abundant in low-albedo regions associated with high thermal inertia (e.g., 0° to 8°N, 350° to 360°W), and they represent a substantial fraction of the probable bedrock exposures in the study area (Fig. 6, lined pattern). The eroded layers are candidates for the surface manifestation of indurated sediments that contribute to the "block" abundance determined from global thermal data (*Jakosky and Christensen,* 1986).

High-resolution thermal infrared data provided thermal inertias for individual areas as small as 2×5 km (Fig. 9). The thermal inertias are quite consistent with values obtained from global studies (*Palluconi and Kieffer,* 1981), indicating the martian surface is locally homogeneous on a scale ranging from hundreds of kilometers down to a few kilometers (*Zimbelman and Leshin,* 1987). A few locations with localized thermal inertia enhancements also correspond to areas of enhanced

bedrock exposure (e.g., 10°S, 345°W). These very localized enhancements are associated with fresh impact craters where interior walls have not been subdued by downslope movement of debris.

Differences between the temperatures measured by the IRTM at 20 μm and 11 μm for the nighttime high-resolution sequences (the diagonal tracks in Fig. 9) show little variation in the abundance of unresolved competent materials, equivalent to "block" abundances of 10% or less over much of the study area. The only exceptions to this trend are five isolated spots (less than or equal to the 15×15 km bin size used in analyzing the data) where "block" values of 15% appear in strong contrast with their surroundings. All five of these locations occur in low-albedo regions with relatively high thermal inertia (5°N to 5°S latitude, 350° to 356°W longitude) and with an abundance of eroded layers visible in nearby images. Unfortunately none of the locations of enhanced "block" abundance is included within a high-resolution imaging frame, but it seems most probable that the IRTM is sensing exposures of the indurated materials observed elsewhere in the study area.
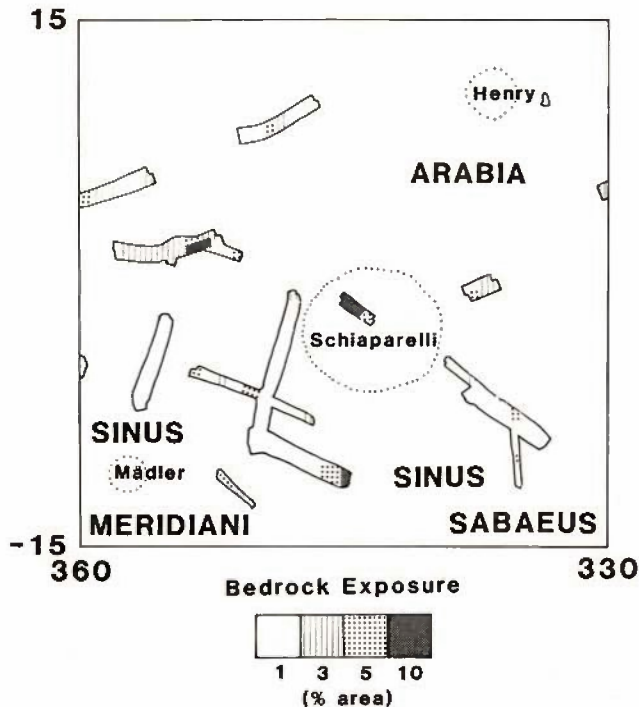
sediments (*Jakosky and Christensen*, 1986). *Presley and Arvidson* (1988) used the thermal infrared spectral technique to document from 1% to about 15% "block" abundances, distributed randomly across the entire area, in the portions of Sinus Meridiani included in this study. The region examined in the present study includes areas that represent almost the entire range of albedos (*Kieffer et al.*, 1977; *Pleskot and Miner*, 1981) and thermal inertias (*Kieffer et al.*, 1977; *Palluconi and Kieffer*, 1981) observed throughout the southern hemisphere of Mars. It seems likely that the results obtained here are applicable to a large portion of the martian surface.

It is important to recognize that the steep slopes examined in this study do not represent the only locations where bedrock might be exposed on the martian surface. It is quite possible that some bedrock materials may be present on more level terrains, with only a slight covering of dust or rocks. Such areas would be essentially impossible to identify from morphologic characteristics, but they could still influence remote-sensing data at visual and, even more strongly, at thermal wavelengths. The close agreement between the overall abundance of unresolved "blocks" of high thermal inertia material (corresponding to rock materials at scales larger than
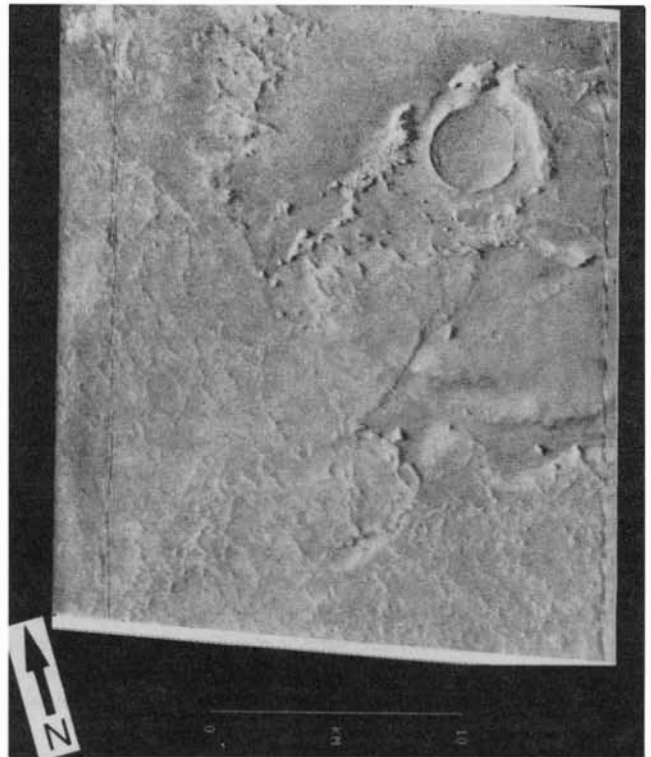
Fig. 7. Footprint map of high-resolution Viking orbiter images examined in this study. Regional albedo features are labeled in capital letters and three named impact craters are indicated by a dotted line along the rim crest. Patterns within the footprints provide a general guide to the spatial distribution of probable bedrock exposures.

There is no correlation between the bedrock exposure estimates obtained from either the images or the high-resolution thermal infrared data when compared with radar reflectance properties for the region (*Downs et al.*, 1975). Regional slopes as inferred from both radar-derived topography (*Downs et al.*, 1982) and global compilation of photogrammetry (*U.S. Geological Survey*, 1989) are low throughout the study area, with typical values much less than 1°. This result is consistent with the observation that areas of probable bedrock exposure occur at localized breaks in slope that are typically much smaller than the areas measured by the topographic techniques given above.

DISCUSSION

How representative is the study area of the martian highlands as a whole? Thermal infrared data obtained at multiple wavelengths indicate that from 5% to 20% of the martian surface consists of material much more competent than either dust or sand, with the low-albedo regions generally having more exposed competent materials than the high-albedo regions (*Christensen*, 1986b). The competent materials observed by this technique may be either rocks approximately 15 cm in diameter (*Christensen*, 1982, 1986b) or indurated

Fig. 8. Example of an eroded layer of competent material, including the exhumation of a buried crater at the upper right, that may not be compositionally related to the underlying bedrock. The competent layer was emplaced on top of the existing topography and is now disintegrating by mechanical and/or chemical weathering processes. Viking Orbiter frame 709A20, centered at 2.2°N, 354.2°W, 20-m/pixel resolution.
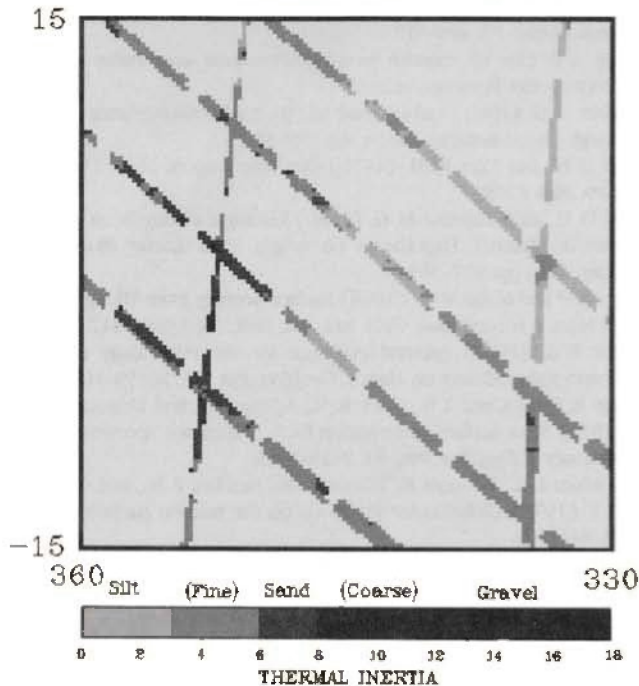
SINUS MERIDIANI REGION

Fig. 9. Thermal inertias determined from high-resolution thermal infrared data collected within the Sinus Meridiani study area. Thermal inertias are related to an effective average particle size (labels above scale) using thermal conductivity information presented in Fig. 10 of *Kieffer et al.* (1977). Overall distribution of values is consistent with results obtained from global mapping but localized enhancements correspond to regions of enhanced bedrock exposure determined from the high-resolution images.

CONCLUSIONS

The following conclusions were obtained from this study of the Sinus Meridiani region: (1) Visual estimates of bedrock exposure in high-resolution images are comparable in total range, but variable in spatial location, to values obtained by nonimaging remote sensing techniques. The spatial variability in exposed bedrock between this study and other techniques is most likely due to large differences in spatial resolution. It is likely that picture elements can include mixtures of competent materials and aeolian dust or sand, making the results obtained from the images representative of probable bedrock exposure on scales larger than tens of meters. (2) The occurrence of probable bedrock exposure is correlated with features that appear to be morphologically recent; this is particularly true for the inner walls of fresh impact craters. This implies that bedrock exposures larger than hundreds of meters may be subdued within periods that are short on a geologic timescale. (3) The spatial distribution of enhanced bedrock exposures is uncorrelated with unit boundaries derived from either spectral reflectance studies or photogeologic mapping. Surface exposures of bedrock may be more the product of geologic processes active on the surface than of the events that formed the large-scale physiographic provinces. (4) It is unlikely that the remote-sensing data presently available for the Sinus Meridiani region provide information that can be directly related to the bedrock properties of regionally extensive geologic units.

10 cm) and the abundance of probable bedrock exposures obtained in the present study (corresponding to scales larger than tens of meters) is particularly important. It is very unlikely that large portions of the study region could consist of bedrock exposures in level terrains (and thus be excluded from our study) without producing a distinct increase in the "block" abundance, either in the high-resolution data (discussed above) or on a regional scale (*Presley and Arvidson*, 1988). This conclusion only strengthens the argument that the compositional inferences obtained from reflectance studies, including low-albedo regions, are relevant to soils and small rocks rather than substantial exposures of bedrock material.

Concentrations of competent materials may be higher than these values at other locations on Mars, such as the upper walls of Valles Marineris or in portions of the southern cratered highlands where unconsolidated materials have been more thoroughly removed from the surface and transported into the northern hemisphere, as proposed by *Christensen* (1986a). Continued identification of candidate bedrock exposures on the martian surface will provide important information for the interpretation of data obtained by the Mars Observer mission, as well as for the selection of possible landing sites for future manned and unmanned missions to Mars.

REFERENCES

Adams J. B. and McCord T. B. (1969) Mars: Interpretation of spectral reflectivity of light and dark regions. *J. Geophys. Res., 74,* 4851-4856.

Arvidson R. E., Guinness E. A., and Zent A. P. (1982) Classification of surface units in the equatorial region of Mars based on Viking Orbiter color, albedo, and thermal data. *J. Geophys. Res., 87,* 10149-10157.

Bell J. F. III, McCord T. B., and Owensby P. D. (1990) Observational evidence of crystalline iron oxides on Mars. *J. Geophys. Res., 95,* 14447-14462.

Best M. G. (1982) *Igneous and Metamorphic Petrology.* Freeman, San Francisco. 630 pp.

Breed C. S., McCauley J. F., and Davis P. A. (1987) Sand sheets of the eastern Sahara and ripple blankets on Mars. In *Desert Sediments: Ancient and Modern* (L. Fostick and I. Ried, eds.), pp. 337-359. Geol. Soc. Am. Spec. Publ. No. 35.

Carr M. H. (1981) *The Surface of Mars.* Yale Univ., New Haven. 232 pp.

Christensen P. R. (1982) Martian dust mantling and surface composition: Interpretation of thermophysical properties. *J. Geophys. Res., 87,* 9985-9998.

Christensen P. R. (1983) Eolian intracrater deposits on Mars: Physical properties and global distribution. *Icarus 56,* 496-518.

Christensen P. R. (1986a) Regional dust deposits on Mars: Physical properties, age, and history. *J. Geophys. Res., 91,* 3534-3546.

Christensen P. R. (1986b) The spatial distribution of rocks on Mars. *Icarus*, *68*, 217-238.

Christensen P. R. and Kieffer H. H. (1979) Moderate resolution thermal mapping of Mars: The channel terrain around the Chryse basin. *J. Geophys. Res.*, *84*, 8233-8238.

Craddock R. A. (1987) High resolution thermal infrared mapping of martian outflow and fretted channels. M.S. thesis, Arizona State Univ., Tempe. 100 pp.

Craddock R. A. and Maxwell T. A. (1990) Resurfacing of the martian highlands in the Amenthes and Tyrrhena region. *J. Geophys. Res.*, *95*, 14265-14278.

Ditteon R. (1982) Daily temperature variations on Mars. *J. Geophys. Res.*, *87*, 10197-10214.

Downs G. S., Reichley P. E., and Green R. R. (1975) Radar measurements of martian topography and surface properties: The 1971 and 1973 oppositions. *Icarus*, *26*, 273-312.

Downs G. S., Mouginis-Mark P. J., Zisk S. H., and Thompson T. W. (1982) New radar-derived topography for the northern hemisphere of Mars. *J. Geophys. Res.*, *87*, 9747-9754.

Greeley R. and Guest J. E. (1987) Geologic map of the eastern equatorial region of Mars. *U.S. Geol. Surv. Map I-1802-B*.

Jakosky B. M. and Christensen P. R. (1986) Global duricrust on Mars: Analysis of remote sensing data. *J. Geophys. Res.*, *91*, 3547-3559.

Kahn R., Guinness E., and Arvidson R. (1986) Loss of fine-scale surface texture in Viking Orbiter images and implications for the inferred distribution of debris mantles. *Icarus*, *66*, 22-38.

Kieffer H. H., Martin T. Z., Peterfreund A. R., Jakosky B. M., Miner E. D., and Palluconi F. D. (1977) Thermal and albedo mapping of Mars during the Viking primary mission. *J. Geophys. Res.*, *82*, 4249-4291.

King J. S. (1977) Geologic map of the Arabia quadrangle of Mars. *U.S. Geol. Surv. Map I-996*.

McCord T. B., Singer R. B., Hawke B. R., Adams J. B., Evans D. L., Head J. W., Mouginis-Mark P. J., Pieters C. M., Huguenin R. L., and Zisk S. H. (1982) Mars: Definition and characterization of global surface units with emphasis on composition. *J. Geophys. Res.*, *87*, 10129-10148.

McEwen A. S. (1987) Mars as a planet (abstract). In *Lunar and Planetary Science XVIII*, pp. 612-613. Lunar and Planetary Institute, Houston.

Moncrief S. R. K. and Williams S. H. (1989) Geologic catalog of high-resolution Viking orbiter images and an alternative origin for dark talus streaks on Mars (abstract). In *Papers Presented at the Fifth Annual Summer Intern Conference*, pp. 16-17. Lunar and Planetary Institute, Houston.

Moore H. J. (1980) Geologic map of the Sinus Sabaeus quadrangle of Mars. *U.S. Geol. Surv. Map I-1196*.

Morris R. V., Gooding J. L., Lauer H. V., and Singer R. B. (1990) Origins of Marslike spectral and magnetic properties of a Hawaiian palagonitic soil. *J. Geophys. Res.*, *95*, 14427-14434.

Mouginis-Mark P. J. (1987) Water or ice in the martian regolith?: Clues from rampart craters seen at very high resolution. *Icarus*, *71*, 268-286.

Mouginis-Mark P. J., Zisk S. H., and Downs G. S. (1980) Characterization of martian surface materials from Earth-based radar: The Memnonia Fossae region. *Proc. Lunar Planet. Sci. Conf. 11th*, pp. 823-838.

Palluconi F. D. and Kieffer H. H. (1981) Thermal inertia mapping of Mars from 60°S to 60°N. *Icarus*, *45*, 415-426.

Peterfreund A. R. (1981) Visual and infrared observations of wind streaks on Mars. *Icarus*, *45*, 447-467.

Pieters C. M. (1989) Seeing through the dust and alteration products of Mars (abstract). In *Lunar and Planetary Science XX*, pp. 850-851. Lunar and Planetary Institute, Houston.

Pleskot L. K. and Miner E. D. (1981) Time variability of martian bolometric albedo. *Icarus*, *45*, 179-201.

Presley M. and Arvidson R. E. (1988) Nature and origin of materials exposed in the Oxia Palus-Western Arabia-Sinus Meridiani region, Mars. *Icarus*, *75*, 499-517.

Sabins F. F. (1978) *Remote Sensing: Principles and Interpretation*. Freeman, San Francisco. 426 pp.

Schaber G. G. (1980) Radar, visual and thermal characteristics of Mars: Rough planar surfaces. *Icarus*, *42*, 159-184.

Scott D. H. and Carr M. H. (1978) Geologic map of Mars. *U.S. Geol. Surv. Map I-1083*.

Scott D. H. and Chapman M. G. (1989) Geologic setting of an unusual martian channel: Hypotheses on origin. *Proc. Lunar Planet. Sci. Conf. 19th*, pp. 377-382.

Sharp R. P. and Malin M. C. (1984) Surface geology from Viking landers on Mars: A second look. *Geol. Soc. Am. Bull.*, *95*, 1398-1412.

Singer R. B. (1982) Spectral evidence for the mineralogy of high-albedo soils and dust on Mars. *J. Geophys. Res.*, *87*, 10159-10168.

Singer R. B., McCord T. B., Clark R. N., Adams J. B., and Huguenin R. L. (1979) Mars surface composition from reflectance spectroscopy: A summary. *J. Geophys. Res.*, *84*, 8415-8426.

Soderblom L. A., Edwards K., Eliason E. M., Sanchez E. M., and Charette M. P. (1978) Global color variations on the martian surface. *Icarus*, *34*, 446-464.

Strickland E. L. (1989) Physical properties of Meridiani Sinus-type units in the central equatorial region of Mars (abstract). In *Lunar and Planetary Science XX*, pp. 1077-1078. Lunar and Planetary Institute, Houston.

Swann G. A., Bailey N. G., Batson R. M., Freeman V. L., Hait M. H., Head J. W., Holt H. E., Howard K. A., Irwin J. B., Larson K. B., Muehlberger W. R., Reed V. S., Rennilson J. J., Schaber G. G., Scott D. R., Silver L. T., Sutton R. L., Ulrich G. E., Wilshire H. G., and Wolfe E. W. (1972) Preliminary geologic investigation of the Apollo 15 landing site. In *Apollo 15 Preliminary Science Report*, pp. 5-1 to 5-112. NASA SP-289.

Thomas P. (1984) Martian intracrater splotches: Occurrence, morphology, and colors. *Icarus*, *57*, 205-227.

Thompson T. W., Masursky H., Shorthill R. W., Tyler G. L., and Zisk S. H. (1974) A comparison of infrared, radar, and geologic mapping of lunar craters. *Moon*, *10*, 87-117.

Thompson T. W., Cutts J. A., Shorthill R. W., and Zisk S. H. (1980) Infrared and radar signatures of lunar craters: Implications about crater evolution. *Proceedings of the Conference on the Lunar Highlands Crust* (J. J. Papike and R. B. Merrill, eds.), pp. 483-499. Pergamon, New York.

U.S. Geological Survey (1989) Topographic maps of the western, eastern equatorial and polar regions of Mars. *U.S. Geol. Surv. Misc. Inv. Ser. Map I-2030*.

Webster's Third New International Dictionary (1971) Merriam, Springfield, Massachusetts.

Wilhelms D. E. (1984) Moon. In *The Geology of the Terrestrial Planets*, pp. 107-205. NASA SP-469.

Zimbelman J. R. (1986) Geologic interpretation of remote sensing data for the martian volcano Ascraeus Mons. In *Advances in Planetary Geology*, pp. 271-572. NASA TM-88784.

Zimbelman J. R. (1987) Spatial resolution and the geologic interpretation of martian morphology: Implications for subsurface volatiles. *Icarus*, *71*, 257-267.

Zimbelman J. R. and Kieffer H. H. (1979) Thermal mapping of the north equatorial and temperate latitudes of Mars. *J. Geophys. Res.*, *84*, 8239-8251.

Zimbelman J. R. and Greeley R. (1981) High resolution visual, thermal, and radar observations in the northern Syrtis Major region of Mars. *Proc. Lunar Planet. Sci. 12B*, pp. 1419-1429.

Zimbelman J. R. and Greeley R. (1982) Surface properties of ancient cratered terrain in the northern hemisphere of Mars. *J. Geophys. Res.*, *87*, 10181-10189.

Zimbelman J. R. and Leshin L. A. (1987) A geologic evaluation of thermal properties for the Elysium and Aeolis quadrangles of Mars. *Proc. Lunar Planet. Sci. Conf. 17th*, in *J. Geophys. Res., 92*, E588-E596.

Zimbelman J. R., Clifford S. M., and Williams S. H. (1989) Concentric crater fill on Mars: An aeolian alternative to ice-rich mass wasting. *Proc. Lunar Planet. Sci. Conf. 19th*, pp. 397-407.